



# Gaze-Evoked Deformations in Optic Nerve Head Drusen

## *Repetitive Shearing as a Potential Factor in the Visual and Vascular Complications*

Patrick A. Sibony, MD,<sup>1</sup> Junchao Wei, PhD,<sup>2</sup> Ian A. Sigal, PhD<sup>2,3</sup>

**Purpose:** To determine if ocular ductions deform intrapapillary and peripapillary tissues in optic nerve head drusen (ONHD) and to compare these deformations with healthy eyes and eyes with other optic neuropathies.

**Design:** Observational case series.

**Participants:** Twenty patients with ONHD.

**Methods:** Axial rasters of the optic nerve from a spectral-domain OCT device (Cirrus 5000; Carl Zeiss Meditec, Inc, Dublin, CA) were used to analyze the shape of the peripapillary basement membrane (ppBM) layer in 20 confirmed cases of ONHD. We compared registered images obtained from 2 eye positions: 10° to 15° in adduction and 30° to 40° in abduction. Geometric morphometrics was used to analyze the shape of the ppBM layer defined by placing 10 equidistant landmarks extending 2500 μm on both sides of the basement membrane opening. We also adapted an image strain tracking technique to measure regional intrapapillary strains in 6 patients. Using manually placed nodes on the reference image (in adduction), an iterative, block-matching algorithm is used to determine local displacements between the reference and its paired image in abduction. Displacement vectors were used to calculate the mean shear and effective strain (percent change).

**Main Outcome Measures:** Peripapillary shape deformations, intrapapillary shear strains, and effective strains.

**Results:** We found a statistically significant difference in the shape of the ppBM layer between abduction and adduction ( $P < 0.01$ ). The deformation was characterized by a relative posterior displacement temporally in adduction that reversed in abduction. Strain tracking in all 6 patients showed substantial gaze-induced shearing and effective strains. Mean effective strains were 7.5% outside the drusen. Shear and effective strains were significantly larger outside versus within the drusen ( $P < 0.003$  and  $P < 0.01$ , respectively).

**Conclusions:** This study demonstrates that horizontal ocular ductions induce significant shearing deformations of the peripapillary retina and prelaminar intrapapillary tissues. We also found that the deformations in healthy persons are similar in magnitude to ONHD. Based on these findings, we speculate that patients with intrapapillary calcifications exposed to the long-term effects of repetitive shearing (induced by ocular ductions) may contribute to the progressive axonal loss and vascular complications associated with ONHD. *Ophthalmology* 2018;125:929-937 © 2018 by the American Academy of Ophthalmology



Supplemental video available at [www.aaojournal.org](http://www.aaojournal.org).

Pseudopapilledema with optic nerve head drusen (ONHD) are intrapapillary calcifications that range in size between 5 and 1000 μm. Early on, buried deep within the prelaminar optic nerve head (ONH), they may not be seen ophthalmoscopically but gradually will become visible as they enlarge and approach the surface. The associated elevation and blurring of the disc can be confused with papilledema. Optic nerve head drusen are associated with a slowly progressive loss of peripheral vision and, rarely, acute vision loss resulting from neuroretinal vascular complications.<sup>1-6</sup>

Using spectral-domain OCT, we and others recently have shown that horizontal ocular ductions induce deformations

of the ONH and peripapillary tissues in healthy participants,<sup>7-9</sup> in those with anterior ischemic optic neuropathy (AION), and in those with papilledema.<sup>7</sup> These studies led us to consider whether stress and strain on the ONH induced by ocular ductions may be a factor in the progressive loss of visual field and vascular complications of ONHD. Our goals were to determine if ocular ductions deform intrapapillary and peripapillary tissues in patients with ONHD using shape analysis and strain tracking techniques, to compare these deformations with previously published data in healthy persons and patients with other optic neuropathies, and to consider the role of gaze-evoked strains in the evolution and complications of ONHD.

## Methods

### Inclusion Criteria

The diagnosis of ONHD was based on the typical ophthalmoscopic features that included visible intrapapillary deposits in most cases, sometimes associated with elevation of the optic disc; vascular anomalies; and peripapillary retinal pigment epithelial changes. Regardless of whether drusen were visible or buried, all patients underwent a B-scan or fundus autofluorescence photography that confirmed the diagnosis. All patients demonstrated OCT findings consistent with the diagnostic criteria defined by the Optic Disc Drusen Studies Consortium recommendations.<sup>10</sup> We excluded any patient with a coexistent disc anomaly (e.g., pseudopapilledema without drusen, tilted optic disc, high myopia, staphylomas, or otherwise dysplastic conditions), optic neuropathies, or papilledema. This study was approved and complied with policies of the State University of New York Stony Brook Committee on Research Involving Humans and complied with the tenets of the Declaration of Helsinki and the Health Insurance Portability and Accountability Act.

### Image Acquisition

A Cirrus 5000 SD-OCT device (Carl Zeiss Meditec, Inc., Dublin, CA) was used to acquire (1) a  $200 \times 200$  optic disc cube and (2) a 5-line, high-definition axial raster (9 mm in length at 0.125-mm intervals) with a signal strength of 7 or more. The optic disc cube was used to calculate the mean retinal nerve fiber layer thickness. The Cirrus 5000 SD-OCT produces vertically stretched raster images with an aspect ratio of 3:2 ( $750 \times 500$  pixels; Fig 1). We corrected the aspect ratio from 3:2 to an unstretched aspect ratio of 9:2 ( $750 \times 167$  pixels) for shape analysis. To illustrate small differences, some of the figures are displayed in a stretched or 3:2 aspect ratio where indicated.

High-definition 5-line axial rasters were obtained in 2 head positions with the eyes in adduction and abduction to the extent

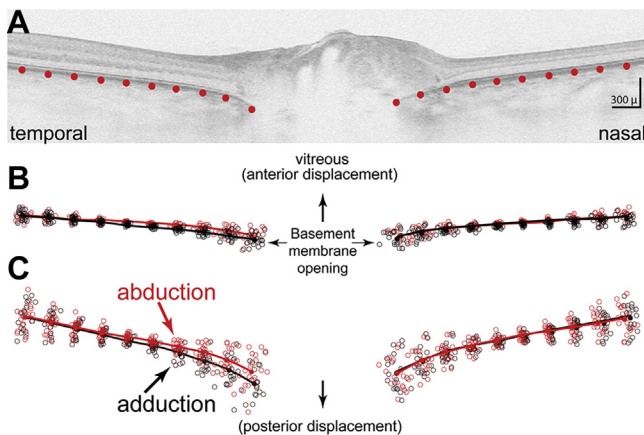


**Figure 1.** A, Diagram showing placement of 10 equidistant semilandmarks spanning 2500  $\mu\text{m}$  on both sides of the basement membrane opening. B, Scatterplot showing semilandmarks from each participant in abduction (red circles) and adduction (black circles) after normalizing for location, size, and rotation (Procrustes superimposition). The lines show the mean (consensus) shapes for each group (black for adduction, red for abduction). C, Three-fold vertically stretched image illustrating differences in more detail. Overall, the shape in adduction is posteriorly displaced temporally relative to the nasal side compared with abduction, which is displaced more anteriorly. The difference in shapes between abduction and adduction was statistically significant ( $P < 0.01$ ).

that the patient and the fixed camera device would permit. Adduction was limited by the patient's nose against the lens element of the device at approximately  $10^\circ$  to  $15^\circ$  and abduction was less restricted at approximately  $30^\circ$  to  $40^\circ$ . These ranges were based on rotational head positions while the patient viewed the OCT fixation target using a head-mounted protractor. Scanning laser ophthalmoscopic image stabilization (FastTrac; Carl Zeiss Meditec, Inc, Dublin, CA) was used to register images. We used the most centrally positioned raster of the 5 raster lines in adduction as a baseline reference to compare with the axial raster obtained in abduction at the same location (Tracked to Prior option). Images were mirrored horizontally when necessary to align the temporal and nasal regions.

### Geometric Morphometric Shape Analysis

We used geometric morphometrics to analyze the shape of the peripapillary basement membrane (ppBM) layer imaged on the spectral-domain OCT raster. This is a well-established method that quantifies and analyzes shape and its covariation with other variables.<sup>11–14</sup> The methodologies are detailed in a primer by Zelditch et al.<sup>14</sup> Additional references and software can be found online at <http://life.bio.sunysb.edu/morph>.<sup>13</sup> The application of this technique to the analysis of the ONH has been described in several previous publications.<sup>7,15–17</sup> The tps software<sup>13</sup> was used in this analysis. A brief description follows.

Geometric morphometrics define shape as that geometric property that remains after normalizing for differences in centroid location, scale, and rotation. Shapes are defined by a series of landmarks whose coordinates are treated as row vectors. Each shape vector can be represented as a distance-based variable, at a single location in a multidimensional space that can be analyzed statistically.

Regarding digitizing semilandmarks, we superimposed a 2500- $\mu\text{m}$  rectilinear grid on the temporal and nasal side of the basement membrane opening (BMO) of a 9-mm axial raster image (unstretched [9:2] aspect ratio) using imaging software (Photoshop; Adobe Systems, San Jose, CA). The grid was used to position 10 equidistant semilandmarks (defined as landmarks placed along a curve or surface) a distance of 2500  $\mu\text{m}$  from the edge of the basement membrane layer on both sides of the BMO. Each semilandmark was positioned along the outer edge of the ppBM layer starting at the edge of the BMO (Fig 1A). Semilandmark placement was performed on image files that were de-identified with respect to name and eye position.

Generalized Procrustes analysis or Procrustes superimposition is a normalization process of superimposing all of the specimen shapes onto a mean shape in 3 sequential steps: first by translating the centroid of the semilandmarks to a single point of origin, then rescaling to a uniform size, and finally minimizing rotational differences between corresponding landmarks.

The thin plate spline displays differences in shape as a smooth deformation using an algorithm that interpolates differences between landmarks and can be visualized using vectors at each landmark. The thin plate spline also defines a set of shape variables (partial warps) that capture the differences between shapes. The partial warp scores generate data matrices that can be analyzed with the proper degrees of freedom using multivariate statistical methods.

Principal component analysis is used to identify and ordinate the variation in shape along a series of components that are linear combinations of the partial warps. In effect, principal component analysis identifies the important patterns of shape based on variance to determine if they distinguish patient groups (in this case, shape differences between abduction and adduction). The relative contribution of each principal component is expressed as a percent of the total variance. Principal component analysis was performed using a variance–covariance matrix of the shape variables.

Statistical analysis of shape is based on comparing the sums of squared Procrustes differences between and within the samples expressed as an  $F$  ratio. The evaluation compares the observed  $F$  value to a distribution based on 10 000 random permutations of the individuals to the groups being compared. The proportion of Goodall's  $F$  statistics from these permutations equal to or larger than the observed Goodall's statistic is interpreted as the  $P$  value for the test. To avoid correlation bias between eyes within an individual, all statistical analyses on shape were performed on the right eye or in unilateral cases the affected eye. A Student  $t$  test was used to compare the means of continuous variables. Analyses of variance were used to complete multiple comparisons of continuous variables.

## Strain Tracking

We adapted recently developed image-tracking techniques to measure local deformations (strains) between abduction and adduction in 6 of our patients for whom intrapapillary image quality permitted. The methods are detailed elsewhere.<sup>18–20</sup> Briefly, the source image in abduction was brought into rough registration with the target image (in adduction) using a rigid body transformation. Next, a set of discrete landmarks was placed manually on the target to use as reference locations for registration between the images. An iterative block-matching algorithm minimizing the zeroed normalized cross-correlation function then was applied to determine the local displacement vectors that bring a block surrounding the landmarks of interest from the source into optimal coincidence with the target. The image matching then was refined using a subpixel phase correlation based on paired image subregions. From the resulting discrete vector field, the full-field displacement and strain tensor were computed and interpolated.

Tissues can be stretched, compressed, or sheared, sometimes simultaneously, in various directions. For simplicity, we focused on shear strains and effective shear strains. Shear strains were chosen because they are a major factor in neural tissue damage.<sup>21,22</sup> Effective strains are convenient because they summarize the multidimensional state of strain into a single value, taking into account tension, compression, and shear.<sup>9</sup> Effective strains also are helpful to compare with previous ONH tracking studies.<sup>9</sup> Effective strains were computed using the methodology of Wang et al.<sup>9</sup> For analysis, images were unstretched by expanding them laterally by a factor of 3. For presentation, they were stretched again by the reverse process.<sup>23</sup> For each participant, 2 regions of interest were defined manually: 1 within the drusen and another outside. The mean shear and effective strains within the regions were computed and compared via paired  $t$  test.

## Results

We identified 20 patients with ONHD. There were 16 females and 6 males with a mean age of  $32 \pm 15$  years (range, 16–55 years). Fourteen of the patients had bilateral ONHD and 6 had unilateral ONHD, and the ONHD were visible in 15 of the patients and buried in 5 patients.

Figure 1B shows a scatterplot of normalized landmarks after Procrustes superimposition from each participant in abduction (red circle) and adduction (black circle). The continuous lines show the mean (consensus) shapes in abduction (black) and adduction (red). Because the differences were small, the image is stretched vertically 3-fold (Fig 1C) to illustrate the change in more detail. Relative to abduction, the shape in adduction is displaced posteriorly on the temporal side of the BMO relative to the nasal side. The pattern in abduction is reversed. The

difference in the mean shape between abduction and adduction was statistically significant to a level of  $P < 0.01$  (permutation).

To characterize those features that best distinguish the shape differences in eye position, we performed a principal component analysis on a variance–covariance matrix of the shape variables derived from the semilandmark data (Fig 2). The first 3 principal components accounted for 90% of the variance in shape. Principal component 1, accounting for 70% of the variance, implied a shape characterized by an anterior (toward vitreous)—posterior (away from vitreous) axial displacement of the ppBM layer. Principal component 2 accounted for 12% of the variance, capturing differences in the diameter of the basement membrane opening. Principal component 3 accounted for 8% of the variance and was characterized by a seesaw tilting with posterior displacement temporally and slight anterior displacement nasally on the positive side of the ordinate. The reverse pattern was depicted on the negative side of the ordinate.

Principal component 3 was the 1 component that most clearly distinguished the shapes associated with abduction and adduction. Although there was considerable overlap in shapes across participants, paired comparisons of each participant showed a consistent pattern in which all but 3 of the patients displayed a positive shift along the ordinate when going from abduction to adduction. Said differently, most patients in abduction had a relative anterior displacement temporally (toward the vitreous, relative negative position on the ordinate) that on adduction shifted posteriorly (away from the vitreous, positively along the ordinate). A symmetrical relative posterior shift in adduction also was seen in principal component 1. There was no clear distinction between abduction and adduction with respect to principal component 2.

An example of an axial raster from one of the participants showing a slight relative posterior displacement temporally is shown in Figure 3. A video clip from another participant is shown online (Video 1, available at [www.aaajournal.org](http://www.aaajournal.org)). We did not find any correlation between shape or change in shape (deformation) with the mean retinal nerve fiber layer or the size or visibility of the druse.

Strain tracking revealed that the change in gaze caused substantial intrapapillary tissue deformations in all 6 patients studied, as shown in Figure 4. Deformations outside the drusen were significantly larger than within. Shear strains were, on average, 7.6 times larger outside the drusen than within (3.8% vs. 0.5%;  $P < 0.003$ ). Effective strains were, on average, 3.4 times larger outside the drusen than within (7.2% vs. 2.1%;  $P < 0.01$ ).

To compare the shape changes in ONHD with healthy patients and those with other optic neuropathies, we reanalyzed a previously published geometric morphometric shape analysis<sup>7</sup> on healthy persons and those with AION or papilledema and combined them with the patients from this study with ONHD. The methodology for both acquisition and analysis using geometric morphometrics was identical in both studies. We found that the patterns and magnitudes of the deformations in ONHD (Fig 5) showed no significant difference (analysis of variance) among those with AION, healthy persons, and those with drusen; however, all 3 were significantly different from those in persons with papilledema, in whom gaze-induced deformations were greatly exaggerated.

## Discussion

While a number of reports have examined the effects of ocular ductions on the normal ONH,<sup>7–9,24–26</sup> this report examines the effects and potential impact of ocular ductions in patients with ONHD. This study shows that patients with

ONHD display significant gaze-evoked deformations in the shape of the ppBM layer and substantial strains within the prelaminar ONH surrounding ONHD.

The shape pattern (displayed in principal component 3) that best distinguished the effects of ocular ductions was a seesaw type of deformation characterized by a posterior displacement temporally in adduction relative to the nasal side. The pattern

was reversed in abduction. Demer<sup>25</sup> proposed that gaze-evoked deformations in healthy persons are caused by the optic nerve sheath tethering the globe, especially in adduction. It is likely that optic nerve sheath tethering also explains the peripapillary deformations in ONHD.

Strain tracking in all 6 patients studied showed substantial gaze-induced shearing and effective strains (Fig 4)

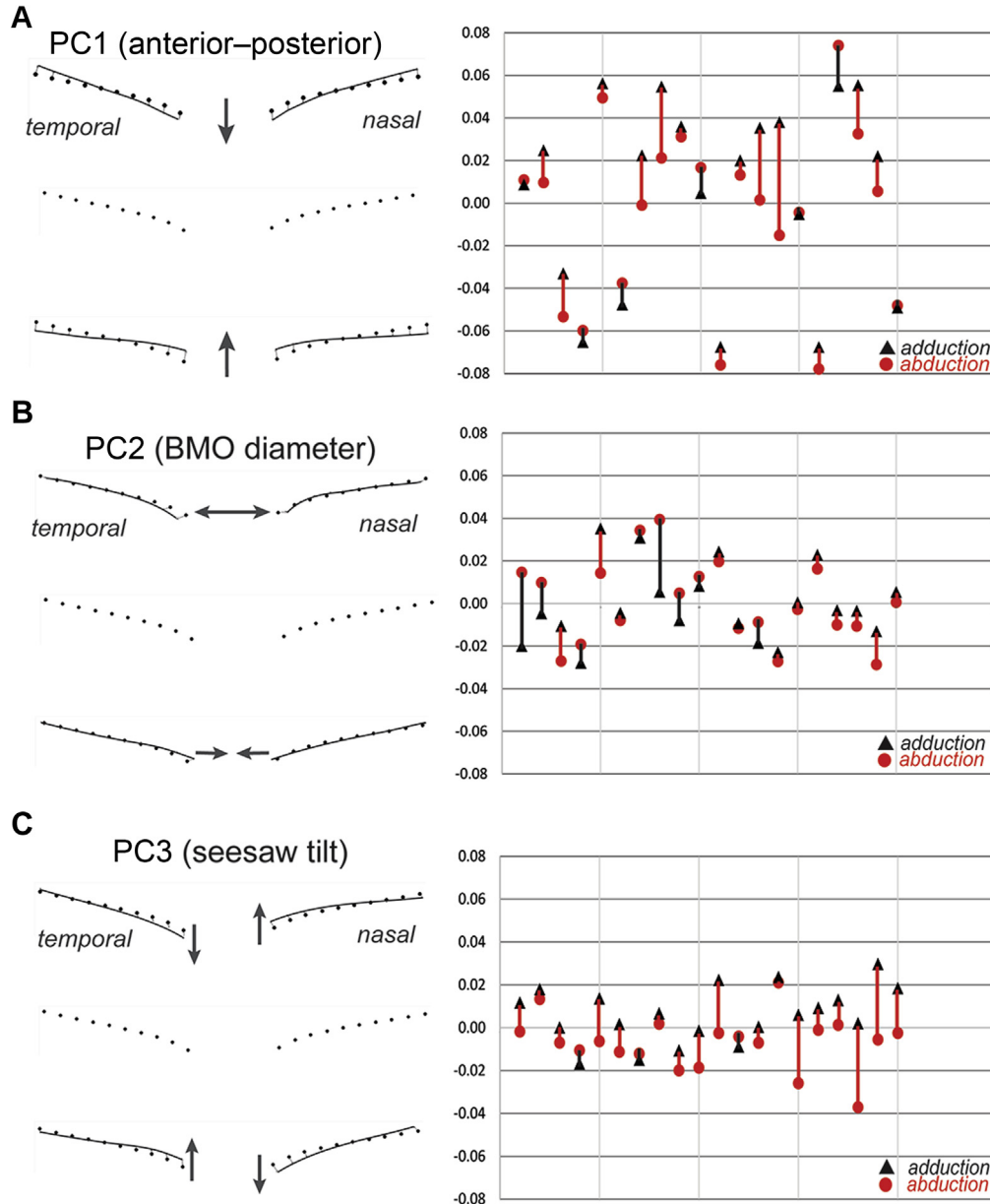


**Figure 2.** Principal component (PC) analysis. The first 3 principal components account for 90% of the variance in shape variables. **A**, Principal component 1 (70%) implies a shape characterized by a symmetrical posterior (away from the vitreous, positive)-to-anterior (toward the vitreous, negative) deformation. **B**, Principal component 2 (12%) depicts the relative diameter of the basement membrane opening. **C**, Principal component 3 (8%) implies a seesaw tilting deformation. The PC scores for each patient along the abscissa represent shapes in abduction (red circles) and adduction (black triangles). A directional line connects each participant pair describing the deformation: positive shifts when going from abduction to adduction are red, and negative shifts are black. Each mark along the ordinate represents 0.100 Procrustes distance units, a measure of shape difference. The larger the difference in shape depicted along the ordinate, the bigger the difference in shape. The PC that most clearly distinguishes the shape difference between abduction and adduction is PC3. A positive shift was noted in 17 of 20 eyes. Thus, when eye position changes from abduction to adduction, the temporal side shifts posteriorly (away from the vitreous) relative to the nasal side. Principal component 1 also shows a relative posterior displacement on adduction in 13 of the patients, although PC1 is more symmetrical than PC3. Principal component 2 is not clearly associated with either abduction or adduction. BMO = basement membrane opening.

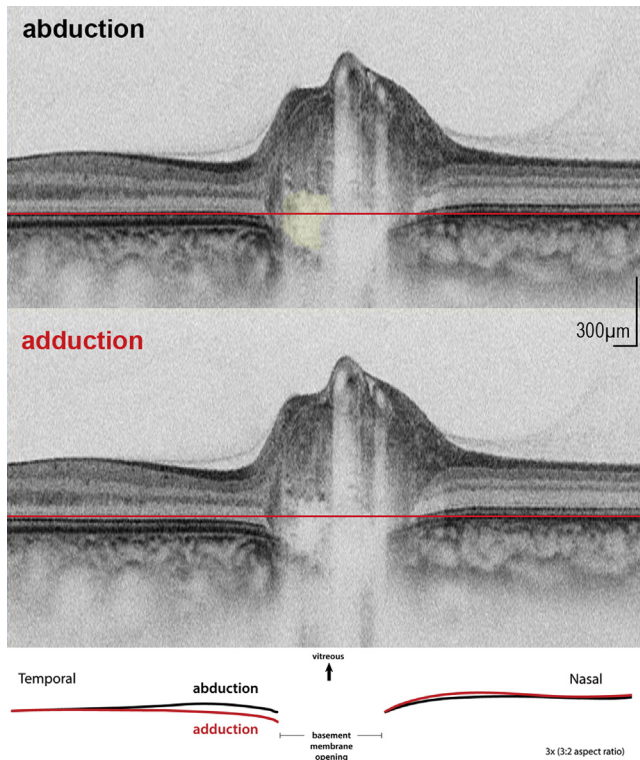


**Figure 3.** Images showing an example in abduction and adduction (vertically stretched image) with inset showing an overlay of the basement membrane layer from each image. Druse appear in yellow in the top figure. Reference plane (red line) shows that in adduction, there is a small posterior displacement temporally relative to the nasal side.

within the prelaminar ONH. Shear and effective strains were significantly larger outside than within the drusen. Mean effective strains of 7.5% outside the drusen in this study were larger than the 5.8% reported by Wang et al<sup>9</sup> as induced within the lamina cribrosa of healthy participants. In 1 individual, shear deformations outside the drusen were more than 18 times larger than within. In the same individual, effective strains outside the drusen reached 14.8%. These findings indicate that, in addition to the deformation of the peripapillary tissues, the prelaminar ONH also is affected by these shearing forces. These results are consistent with the work of others in healthy participants.<sup>7–9,24–26</sup>

The functional impact of ocular ductions on the healthy ONH is unknown. The empirical observations described in this report are consistent with finite element analyses showing alternating gaze-induced strains in the peripapillary sclera, temporally in adduction and nasally in abduction.<sup>24,27</sup> The shape deformations and the strain tracking observed in this study, in addition to those previously reported in healthy persons, suggest that ocular ductions generate a shearing strain within the ONH.<sup>7–9,24,27</sup> Although the magnitude of the deformations in both ONHD patients and healthy participants are similar, the presence of intrapapillary calcifications subjected to repetitive motion strains may damage contiguous axons, glial cells, and blood vessels. For example, fluid–structure interaction models have shown that repetitive pulsatile loads (from blood flow) on microcalcifications in atherosclerotic plaques concentrate enough stress around each microbody to weaken the plaque and cause rupture and thrombosis.<sup>28,29</sup>

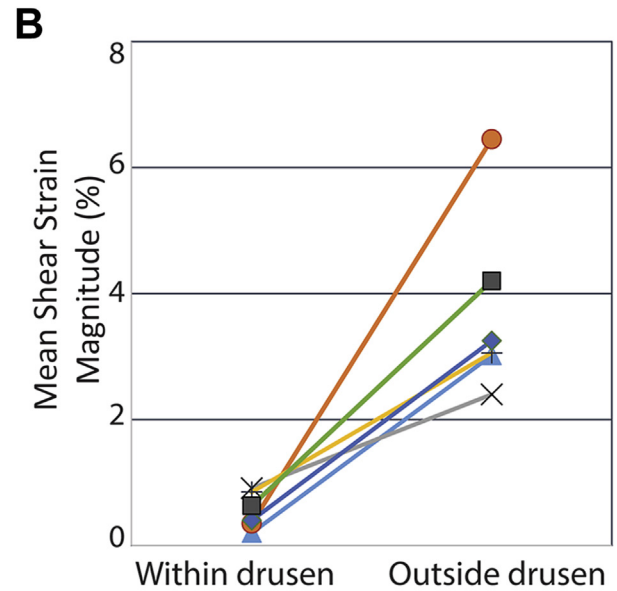
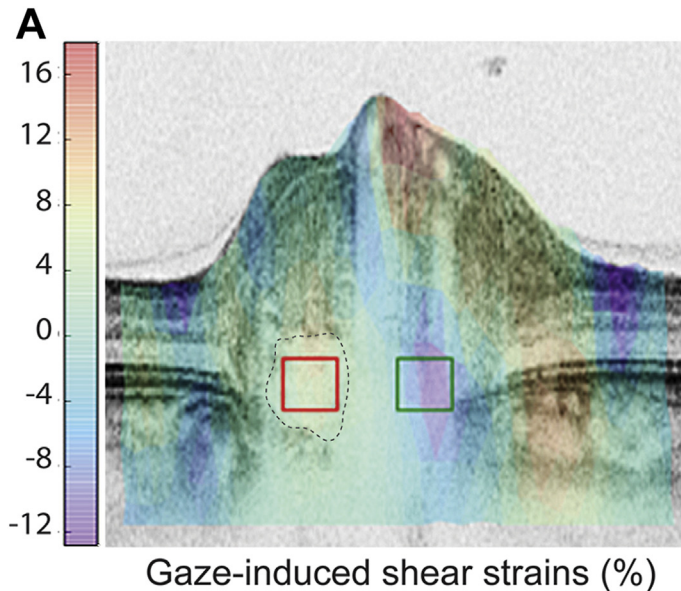


**Figure 4.** Results of tracking analysis to compute the gaze-induced deformations from abduction to adduction. **A**, B-scan of the signature case colored according to the magnitude of the shear deformation. Positive shear is clockwise, whereas negative shear is counter clockwise. Overlaid on the colored OCT are 2 boxes indicating the regions where the strains within (red box) and outside (green box) the druse (dotted outline) were averaged for comparison. Note the smaller deformations within the druse than outside. The large deformations on the vessels are likely the result of pulsation. **B**, Change in gaze caused substantial shear strains outside the drusen, but not within the drusen, in all participants ( $P < 0.003$ , each line is a participant).

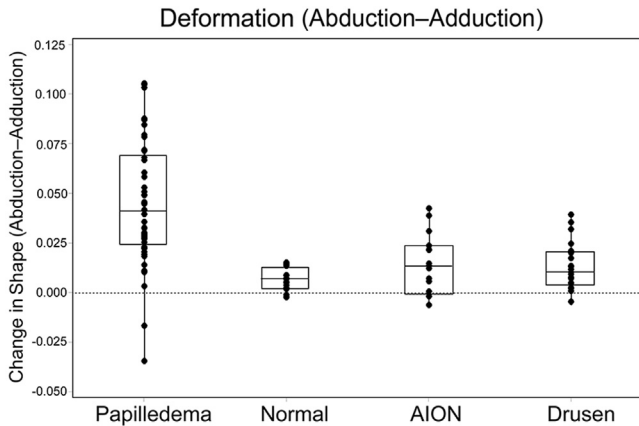


**Figure 5.** Box-and-whisker plot with each point representing the difference in shape (deformation) between abduction and adduction. Consider each point to represent the size and direction of the connecting lines between paired shapes shown in Figure 2. A positive value (along the ordinate) represents a relative posterior displacement temporally or anterior displacement nasally when going from abduction to adduction; a negative value implies the reverse. Most patients showed a positive shift across all groups; however, the magnitude of these shifts varied. Deformations in healthy persons, those with anterior ischemic optic neuropathy (AION), and those with drusen are small compared with the large deformations in papilledema. The differences among those with AION, healthy persons, and those with drusen were not statistically different. The difference between papilledema and the other 3 states was significant ( $P < 0.001$ , analysis of variance). Note that data from papilledema patients, healthy persons, and AION patients has been published previously,<sup>7</sup> but the methodologies for optic nerve head drusen were identical to the other groups. This figure represents a reanalysis of the entire cohort as a group.

The effects of repetitive ocular ductions on ONHD may be analogous.

Repetitive ocular ductions in theory can contribute to axonal injury. A healthy participant executes approximately 150 000 saccades per day and billions over the course of a lifetime.<sup>30</sup> Repetitive motion strains have wide-ranging effects on both tissue<sup>21,22,31</sup> and cell<sup>32–37</sup> functions in a variety of neural and myotendinous disorders.<sup>38</sup> Dynamic stretch injuries of the optic nerve in an animal model have determined that threshold strains of more than 14% can result in histologic and electrophysiologic signs of injury.<sup>39</sup> Repetitive peripapillary scleral strain also may affect blood flow through the branches of the short posterior ciliary arteries that supply the ONH.<sup>40</sup>

The complications of ONHD consist of a progressive loss of visual field, hemorrhages, and vascular occlusions. The prevalence of visual field defects can vary between 24% and 87%.<sup>1,41,42</sup> Visual field loss is slow and progressively declines with age.<sup>43–48</sup> Severity of the field loss correlates with drusen size, surface visibility,<sup>1,42,49–52</sup> mean retinal nerve fiber layer thickness, and ganglion cell layer thickness.<sup>49,52–54</sup> Peripapillary subretinal and flame retinal hemorrhages have been described in 2% to 10% of ONHD. There have been reports associating ONHD with ischemic optic neuropathy, central retinal artery occlusion, central retinal vein occlusion, and choroidal neovascular membranes.<sup>1,55–60</sup> The proposed mechanisms include compressive axonal injury, erosion of blood vessels, ischemic venous congestion, or arteriolar occlusion.<sup>1,2,61,62</sup>

There is strong evidence, by a number of investigators, that the axonal attrition and visual field loss in ONHD is predominantly caused a degenerative axonopathy.<sup>4–6,54,63,64</sup> The present study raises the possibility that repetitive

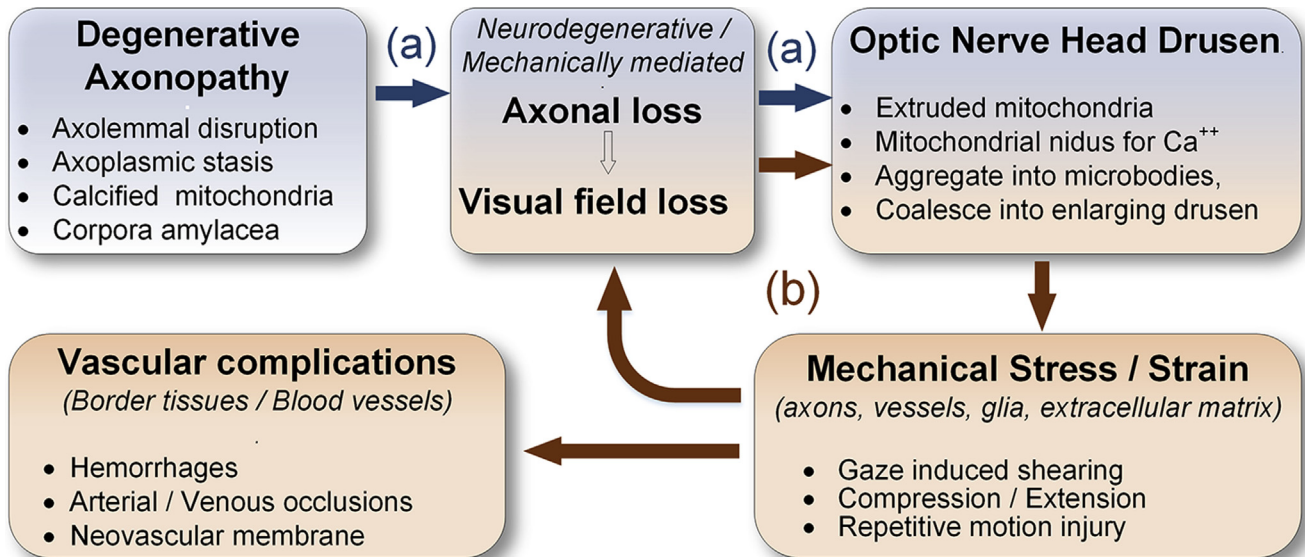


**Figure 6.** Diagram summarizing the hypothetical pathogenesis of optic nerve head drusen formation and complications, which may be mediated by 2 parallel pathways: (a) the first (blue) involves an idiopathic neurodegenerative axonopathy that presumably causes both axon loss and drusen formation; (b) the second (red), involves a progressive increase and enlargement of drusen that may mechanically injure (by shearing, compression) axons and blood vessels causing a cycle of axonal injury, progressive visual field loss and vascular complications. The relative contribution of neurodegenerative and mechanical pathways to the axonal injury, progressive loss of visual fields, and formation of drusen is unknown and may vary at different points in time.

gaze-induced shearing on the ONH also may contribute, in part, to progressive axonal injury and vascular complications of ONHD.

We hypothesize 2 parallel pathways that mediate progressive loss of visual field and axonal attrition in ONHD (Fig 6).<sup>6</sup> The first involves an ill-defined neurodegenerative axonopathy (Fig 6, blue). Seitz<sup>63</sup> and Seitz and Kersting<sup>64</sup> were the first to propose that ONHD are the byproducts of degenerating axons. Spencer<sup>4</sup> speculated that axoplasmic flow is impaired in ONHD.<sup>65,66</sup> Ultrastructural study by Tso<sup>5</sup> and Woodford and Tso<sup>67</sup> demonstrated disruption of the axolemma, calcification of intracellular and extracellular mitochondria, and the formation of corpora amylacea (also containing calcified mitochondria). They proposed that extruded mitochondria serve as nuclei for progressive calcification that eventually coalesce into drusen. The combination of protein deposits and mitochondrial disturbances are characteristic of a variety of neurodegenerative diseases.<sup>4,54</sup>

The second pathway (Fig 6, red) is a mechanical consequence of progressively enlarging intrapapillary calcifications that eventually compress and damage adjacent tissues (i.e., axons, glial cells, blood vessels).<sup>1,2</sup> Repetitive gaze-induced shearing, a previously neglected mechanical component, may be a contributory factor in progressive axonal injury and field loss. Distinctions in the mode and temporal pattern of stress and strain are important because repetitive shearing may be more damaging to tissues than slow compression or extension. Gaze-evoked shearing injury of axons fuels a cycle of axolemmal disruption, mitochondrial extrusion, and progressive calcification that increase the size and number of ONHD. The relative importance of each pathway is unknown, but probably changes with age and ONHD size, number, and location.

Repetitive mechanical shearing around a druse also may damage the border tissues and blood vessels of the ONH. The intermediate tissue of Kuhnt and border tissue of Jacoby are sleeves of glial tissue that provide a barrier cushion between axons of the ONH and retinal and choroidal layers. This region contains small branches of the posterior ciliary artery, the arterial ring of Zinn Haller, and the choroid that supply the prelaminar ONH. Repetitive shearing at the margins of the BMO contiguous to a druse may cause small bleeds that dissect into the frayed margins of the peripapillary tissue planes. Repetitive traumatic shearing in this location also may stimulate the formation of peripapillary choroidal neovascular membranes.

This report has the usual constraints of a retrospective study, including a small sample size. There are also the inherent limitations of OCT, including shadowing and the disadvantages of 2-dimensional imaging compared with volume scans. Most importantly, structural changes do not necessarily reflect clinically significant functional effects. The strengths and limitations of deformation tracking analysis are discussed in detail elsewhere.<sup>18–20</sup> Briefly, deformation tracking is more accurate in regions of high signal quality and low noise. This is important in this work because signal quality decreases quickly with depth in an elevated optic disc. Hence, it was not possible to image the lamina cribrosa consistently. For this reason we focused our analysis of gaze-

induced deformations in the prelaminar region. Finally, there are a number of open questions about the hypothetical model presented in Figure 6, including the root cause of the axonopathy, the relative contributions of neurodegenerative versus biomechanical factors in axonal attrition and field loss, and the long-term consequences of repetitive ocular ductions in ONHD as well as other optic neuropathies.

## References

1. Auw-Haedrich C, Staubach F, Witschel H. Optic disk drusen. *Surv Ophthalmol.* 2002;47:515–532.
2. Friedman AH, Gartner S, Modi SS. Drusen of the optic disc. A retrospective study in cadaver eyes. *Br J Ophthalmol.* 1975;59:413–421.
3. Friedman AH, Henkind P, Gartner S. Drusen of the optic disc. A histopathological study. *Trans Ophthalmol Soc U K.* 1975;95:4–9.
4. Spencer WH. XXXIV Edward Jackson Memorial Lecture: drusen of the optic disc and aberrant axoplasmic transport. *Ophthalmology.* 1978;85:21–38.
5. Tso MO. Pathology and pathogenesis of drusen of the optic nervehead. *Ophthalmology.* 1981;88:1066–1080.
6. Brodsky MC. *Pediatric Neuro-ophthalmology.* 3rd ed. New York: Springer; 2016.
7. Sibony PA. Gaze evoked deformations of the peripapillary retina in papilledema and ischemic optic neuropathy. *Invest Ophthalmol Vis Sci.* 2016;57:4979–4987.
8. Chang MY, Shin A, Park J, et al. Deformation of optic nerve head and peripapillary tissues by horizontal duction. *Am J Ophthalmol.* 2017;174:85–94.
9. Wang X, Beotra MR, Tun TA, et al. In vivo 3-dimensional strain mapping confirms large optic nerve head deformations following horizontal eye movements. *Invest Ophthalmol Vis Sci.* 2016;57:5825–5833.
10. Malmqvist L, Bursztyn L, Costello F, et al. The optic disc drusen studies consortium recommendations for diagnosis of optic disc drusen using optical coherence tomography. *J Neuroophthalmol.* 2017. <https://doi.org/10.1097/WNO.0000000000000585> [Epub ahead of print].
11. Sanfilippo PG, Cardini A, Hewitt AW, et al. Optic disc morphology—rethinking shape. *Prog Retin Eye Res.* 2009;28:227–248.
12. Adams DC, Rohlf FJ, Slice DE. Geometric morphometrics: ten years of progress following the “revolution.” *Ital J Zool.* 2004;71:1,5–16.
13. Rohlf FJ. Morphometrics at SUNY Stony Brook. <http://life.bio.sunysb.edu/morph/>. Accessed December 22, 2017.
14. Zelditch M, Swiderski DL, Sheets HD. *Geometric morphometrics for biologists: a primer.* 2nd ed. San Diego, CA: Elsevier Academic Press; 2012.
15. Sibony P, Kupersmith MJ, Rohlf FJ. Shape analysis of the peripapillary RPE layer in papilledema and ischemic optic neuropathy. *Invest Ophthalmol Vis Sci.* 2011;52:7987–7995.
16. Sibony P, Kupersmith MJ, Honkanen R, et al. Effects of lowering cerebrospinal fluid pressure on the shape of the peripapillary retina in intracranial hypertension. *Invest Ophthalmol Vis Sci.* 2014;55:8223–8231.
17. Sibony P, Strachovsky M, Honkanen R, Kupersmith MJ. Optical coherence tomography shape analysis of the peripapillary retinal pigment epithelium layer in presumed optic

- nerve sheath meningiomas. *J Neuroophthalmol.* 2014;34:130–136.
18. Lall P, Wei J. X-ray micro-CT and DVC based analysis of strains in metallization of flexible electronics. Thermal and Thermomechanical Phenomena in Electronic Systems (ITherm). Orlando, Florida: IEEE Intersociety Conference; 2017. <https://doi.org/10.1109/ITHERM.2017.7992628>.
  19. Tran H, Grimm J, Wang B, et al. Mapping in-vivo optic nerve head strains caused by intraocular and intracranial pressures. *Proc SPIE Optical Elastography and Tissue Biomechanics.* 2017;IV:100670B-1-10.
  20. Sigal IA, Grimm JL, Jan NJ, et al. Eye-specific IOP-induced displacements and deformations of human lamina cribrosa. *Invest Ophthalmol Vis Sci.* 2014;55:1–15.
  21. Sigal IA, Flanagan JG, Tertinegg I, Ethier CR. Predicted extension, compression and shearing of optic nerve head tissues. *Exp Eye Res.* 2007;85:312–322.
  22. Edwards ME, Wang SS, Good TA. Role of viscoelastic properties of differentiated SH-SY5Y human neuroblastoma cells in cyclic shear stress injury. *Biotechnol Prog.* 2001;17:760–767.
  23. Sigal IA, Schuman JS, Ishikawa H, et al. A problem of proportions in OCT-based morphometry and a proposed solution. *Invest Ophthalmol Vis Sci.* 2016;57:484–485.
  24. Wang X, Rumpel H, Lim WE, et al. Finite element analysis predicts large optic nerve head strains during horizontal eye movements. *Invest Ophthalmol Vis Sci.* 2016;57:2452–2462.
  25. Demer JL. Optic nerve sheath as a novel mechanical load on the globe in ocular duction. *Invest Ophthalmol Vis Sci.* 2016;57:1826–1838.
  26. Suh SY, Le A, Shin A, et al. Progressive deformation of the optic nerve head and peripapillary structures by graded horizontal duction. *Invest Ophthalmol Vis Sci.* 2017;58:5015–5021.
  27. Wang X, Fisher LK, Milea D, et al. Predictions of optic nerve traction forces and peripapillary tissue stresses following horizontal eye movements. *Invest Ophthalmol Vis Sci.* 2017;58:2044–2053.
  28. Bluestein D, Alemu Y, Avrahami I, et al. Influence of microcalcifications on vulnerable plaque mechanics using FSI modeling. *J Biomech.* 2008;41:1111–1118.
  29. Rambhia SH, Liang X, Xenos M, et al. Microcalcifications increase coronary vulnerable plaque rupture potential: a patient-based micro-CT fluid-structure interaction study. *Ann Biomed Eng.* 2012;40:1443–1454.
  30. Schiller PH, Tehovnik EJ. Neural mechanisms underlying target selection with saccadic eye movements. *Prog Brain Res.* 2005;149:157–171.
  31. Morrison JC. Integrins in the optic nerve head: potential roles in glaucomatous optic neuropathy (an American Ophthalmological Society thesis). *Trans Am Ophthalmol Soc.* 2006;104:453–477.
  32. Rogers RS, Dharsee M, Ackloo S, et al. Proteomics analyses of human optic nerve head astrocytes following biomechanical strain. *Mol Cell Proteomics.* 2012;11:M111012302.
  33. Kirwan RP, Crean JK, Fenerty CH, et al. Effect of cyclical mechanical stretch and exogenous transforming growth factor-beta1 on matrix metalloproteinase-2 activity in lamina cribrosa cells from the human optic nerve head. *J Glaucoma.* 2004;13:327–334.
  34. Kirwan RP, Fenerty CH, Crean J, et al. Influence of cyclical mechanical strain on extracellular matrix gene expression in human lamina cribrosa cells in vitro. *Mol Vis.* 2005;11:798–810.
  35. Kirwan RP, Wordinger RJ, Clark AF, O'Brien CJ. Differential global and extra-cellular matrix focused gene expression patterns between normal and glaucomatous human lamina cribrosa cells. *Mol Vis.* 2009;15:76–88.
  36. Tan JC, Kalapesi FB, Coroneo MT. Mechanosensitivity and the eye: cells coping with the pressure. *Br J Ophthalmol.* 2006;90:383–388.
  37. Ingber DE. Mechanobiology and diseases of mechanotransduction. *Ann Med.* 2003;35:564–577.
  38. Barr AE, Barbe MF. Pathophysiological tissue changes associated with repetitive movement: a review of the evidence. *Phys Ther.* 2002;82:173–187.
  39. Bain AC, Meaney DF. Tissue-level thresholds for axonal damage in an experimental model of central nervous system white matter injury. *J Biomech Eng.* 2000;122:615–622.
  40. Langham ME. The temporal relation between intraocular pressure and loss of vision in chronic simple glaucoma. *Glaucoma.* 1980;2:427–435.
  41. Mustonen E. Pseudopapilloedema with and without verified optic disc drusen. A clinical analysis II: visual fields. *Acta Ophthalmol (Copenh).* 1983;61:1057–1066.
  42. Savino PJ, Glaser JS, Rosenberg MA. A clinical analysis of pseudopapilledema. II. Visual field defects. *Arch Ophthalmol.* 1979;97:71–75.
  43. Malmqvist L, Hamann S. Photographic documentation of optic disc drusen over more than 50 years. *JAMA Ophthalmol.* 2017;135:e165470.
  44. Malmqvist L, Lund-Andersen H, Hamann S. Long-term evolution of superficial optic disc drusen. *Acta Ophthalmol.* 2017;95:352–356.
  45. Merchant KY, Su D, Park SC, et al. Enhanced depth imaging optical coherence tomography of optic nerve head drusen. *Ophthalmology.* 2013;120:1409–1414.
  46. Spencer TS, Katz BJ, Weber SW, Digre KB. Progression from anomalous optic discs to visible optic disc drusen. *J Neuroophthalmol.* 2004;24:297–298.
  47. Lee AG, Zimmerman MB. The rate of visual field loss in optic nerve head drusen. *Am J Ophthalmol.* 2005;139:1062–1066.
  48. Lansche RK, Rucker CW. Progression of defects in visual fields produced by hyaline bodies in optic disks. *AMA Arch Ophthalmol.* 1957;58:115–121.
  49. Traber GL, Weber KP, Sabah M, et al. Enhanced depth imaging optical coherence tomography of optic nerve head drusen: a comparison of cases with and without visual field loss. *Ophthalmology.* 2017;124:66–73.
  50. Grippo TM, Shihadeh WA, Schargus M, et al. Optic nerve head drusen and visual field loss in normotensive and hypertensive eyes. *J Glaucoma.* 2008;17:100–104.
  51. Wilkins JM, Pomeranz HD. Visual manifestations of visible and buried optic disc drusen. *J Neuroophthalmol.* 2004;24:125–129.
  52. Malmqvist L, Lindberg AW, Dahl VA, et al. Quantitatively measured anatomic location and volume of optic disc drusen: an enhanced depth imaging optical coherence tomography study. *Invest Ophthalmol Vis Sci.* 2017;58:2491–2497.
  53. Malmqvist L, Wegener M, Sander BA, Hamann S. Peripapillary retinal nerve fiber layer thickness corresponds to drusen location and extent of visual field defects in superficial and buried optic disc drusen. *J Neuroophthalmol.* 2016;36:41–45.
  54. Sato T, Mrejen S, Spaide RF. Multimodal imaging of optic disc drusen. *Am J Ophthalmol.* 2013;156:275–282.e1.
  55. Harris MJ, Fine SL, Owens SL. Hemorrhagic complications of optic nerve drusen. *Am J Ophthalmol.* 1981;92:70–76.

56. Mustonen E. Pseudopapilloedema with and without verified optic disc drusen. A clinical analysis I. *Acta Ophthalmol (Copenh)*. 1983;61:1037–1056.
57. Rosenberg MA, Savino PJ, Glaser JS. A clinical analysis of pseudopapilledema. I. Population, laterality, acuity, refractive error, ophthalmoscopic characteristics, and coincident disease. *Arch Ophthalmol*. 1979;97:65–70.
58. Gittinger Jr JW, Lessell S, Bondar RL. Ischemic optic neuropathy associated with optic disc drusen. *J Clin Neuro-ophthalmol*. 1984;4:79–84.
59. Rubinstein K, Ali M. Retinal complications of optic disc drusen. *Br J Ophthalmol*. 1982;66:83–95.
60. Hitchings RA, Corbett JJ, Winkleman J, Schatz NJ. Hemorrhages with optic nerve drusen. A differentiation from early papilledema. *Arch Neurol*. 1976;33:675–677.
61. Brodrick JD. Drusen of the disc and retinal haemorrhages. *Br J Ophthalmol*. 1973;57:299–306.
62. Karel I, Otravec J, Peleska M. Fluorescence angiography in circulatory disturbances in drusen of the optic disk. *Ophthalmologica*. 1972;164:449–462.
63. Seitz R. Die intraokularen Drusen [The intraocular drusen]. *Klin Monatsbl Augenheilkd*. 1968;152:203–211.
64. Seitz R, Kersting G. Der Drusen der Sehnervenpapille und des Pigmentepithels. *Klin Monatsbl Augenheilkd*. 1962;140:75–88.
65. Jonas JB, Gusek GC, Guggenmoos-Holzmann I, Naumann GO. Optic nerve head drusen associated with abnormally small optic discs. *Int Ophthalmol*. 1987;11:79–82.
66. Mullie MA, Sanders MD. Scleral canal size and optic nerve head drusen. *Am J Ophthalmol*. 1985;99:356–359.
67. Woodford B, Tso MO. An ultrastructural study of the corpora amylacea of the optic nerve head and retina. *Am J Ophthalmol*. 1980;90:492–502.

## Footnotes and Financial Disclosures

Originally received: November 6, 2017.

Final revision: November 30, 2017.

Accepted: December 4, 2017.

Available online: January 18, 2018.

Manuscript no. 2017-2533.

<sup>1</sup> Department of Ophthalmology, State University of New York Stony Brook, Stony Brook, New York.

<sup>2</sup> Department of Ophthalmology, University of Pittsburgh, Pittsburgh, Pennsylvania.

<sup>3</sup> McGowan Institute for Regenerative Medicine, University of Pittsburgh, Pittsburgh, Pennsylvania.

Financial Disclosure(s):

The author(s) have no proprietary or commercial interest in any materials discussed in this article.

Supported by the National Eye Institute, National Institutes of Health, Bethesda, Maryland (grant nos.: EY023966 and EY025011).

HUMAN SUBJECTS: Human subjects were included in this study. No animal subjects were used in this study. The State University of New York Stony Brook Committee on Research Involving Humans approved the study. The study was performed in accordance with the tenets of the

Declaration of Helsinki and the Health Insurance Portability and Accountability Act. This study qualified for waiver of consent pursuant to 45 CFR 46.116.d.

Author Contributions:

Conception and design: Sibony

Analysis and interpretation: Sibony, Wei, Sigal

Data collection: Sibony, Sigal

Obtained funding: None

Overall responsibility: Sibony, Wei, Sigal

Abbreviations and Acronyms:

**AION** = anterior ischemic optic neuropathy; **BMO** = basement membrane opening; **ONH** = optic nerve head; **ONHD** = optic nerve head drusen; **ppBM** = peripapillary basement membrane.

Correspondence:

Patrick A. Sibony, MD, Department of Ophthalmology, University Hospital and Medical Center, Health Sciences Center, SUNY Stony Brook, Stony Brook, NY 11794. E-mail: [patrick.sibony@stonybrook.edu](mailto:patrick.sibony@stonybrook.edu).